Analysis of Side-Polished Few-Mode Optical Fiber

Taylor J. Ray

Thesis submitted to the Faculty of the
Virginia Polytechnic Institute and State University
in partial fulfillment of the requirements for the degree of

Master's of Science
in
Electrical Engineering

Anbo Wang, Chair
Xiaoting Jia
Wei Zhou
Yizheng Zhu

April 29, 2019
Blacksburg, Virginia

Keywords: side-polished fiber, few-mode, fiber optics, weakly-guided fiber

Analysis of Side-Polished Few-Mode Optical Fiber

Taylor J. Ray

(ABSTRACT)

Side-polished fiber allows access to the evanescent field propagating in the cladding of a few-mode fiber. This cladding mode is analyzed and experimentally validated to further the design of a novel class of fiber optic devices. Specific modes are excited in the polished fiber using a phase-only spatial light modulator to determine spatial mode distribution. Each mode is excited and compared to the expected field distribution and to confirm that higher order modes can propagate through side-polished fiber. Based on each mode's distribution, a side-polished fiber can be designed so that perturbations on the polished portion of the fiber effect each mode independently. By carefully analyzing the effects of identical perturbations on each mode, it is determined that each mode can be isolated based on the geometry of the polished fiber and careful alignment of the mode field. Since each mode has a different interaction based on the geometry of the polished fiber, the modes can be affected individually to create fiber optic sensors or communication devices. This research has the potential to advance the development of novel fiber-based devices utilizing mode-domain interferometry and mode multiplexing.

Analysis of Side-Polished Few-Mode Optical Fiber

Taylor J. Ray

(GENERAL AUDIENCE ABSTRACT)

Fiber optic devices have seen significant advancement since the realization of the laser and low-loss optical fiber. Modern day fiber optics are commonly utilized for high-bandwidth communications and specialized sensing applications. Utilizing multiple modes, or wave distributions, in a fiber provides significant advantages towards increasing bandwidth for communications and provides potential for more accurate sensing techniques. Significant research has been conducted in both the sensing and communication field, but mode-domain devices have the capability to significantly advance the field of fiber optic devices. This thesis demonstrates the potential for side-polished fiber geometry to effect each mode independently, thus allowing side-polished fiber to be utilized for realizing novel devices such as multiplexing devices and fiber optic sensors.

Dedication

I would like to dedicate this to my family and friends. Especially my parents who have been a constant support through all of my endeavors. I would not be here without you.

Acknowledgments

I would like to acknowledge my advisor, Dr. Anbo Wang, and all of my committee members for their support in completing my degree. Additionally, Dr. Yong Xu for providing funding for the project. I would also like to acknowledge Dr. Islam Ashry and Dr. Dong Wang who provided invaluable insight and assisted me throughout my research.

Contents

List of Figures

List of Tables

List of Abbreviations

CCD charged-coupling device

LP linearly polarized

PD photodetector

SEM scanning electron microscope

SLM spatial light modulator

SPF side-polished fiber

TIR total internal reflection

Chapter 1

Introduction

The development of optical fiber technology has led to numerous technological enhancements in sensing and telecommunications. In the 1960s, two key scientific discoveries led to a surge in fiber optic technology: the laser [1] and the low-loss optical fiber [2].

Initial optical fiber research focused heavily on improvements in telecommunication applications. The development of technologies such as the internet led to a need for increased bandwidth for data communication. Advancements in fiber optics were well suited to this need, but have developed slowly over the years due to high cost compared to traditional copper based systems. Despite high cost, fiber optics have many significant advantages over traditional copper based telecommunication systems. Fiber based systems have greater bandwidth, decreased attenuation, and resilience to electromagnetic interference resulting in higher data transfer speeds, greater efficiency, and more reliable signals. Recent societal trends require greater data transfer bandwidth, which has resulted in developed countries more readily adopting fiber optic telecommunications. In 2004, it was estimated that a global network of over 250,000 km of sub-marine fiber communications cable with a capacity of 2.56 Tb/s was completed [3]. Since then, significant advancements in fiber optic fabrication and operational techniques have decreased cost dramatically allowing for widespread adoption of such technology, especially in developed countries [**?**]. In fact, in some areas of the world where housing density is high, it is estimated to be more cost effective to employ a fiber system rather than a traditional copper based telecommunications network. However, in

many situations it is still more cost effective to utilize an electrical transmission system. To overcome this cost barrier and increase adoption of fiber optic telecommunication, further improvement in fabrication and operational devices is needed to improve bandwidth and decrease cost.

In addition to telecommunications advancements, low-loss optical fibers are utilized for sensor technology. The main drive for fiber optic sensor technology today is producing a range of sensing techniques which are used for a variety of detection purposes. Fiber optic sensors are typically more complicated and expensive than conventional sensor technologies, which means their development typically relies on niche applications [4]. Many optical fiber sensors are designed for situations where conventional sensors are not suited to the environment (i.e. high temperature, high electromagnetic interference, etc.). Additionally, fiber optic sensors are advantageous in that numerous sensors can be multiplexed effectively in a single fiber resulting in robust distributed sensing technologies. These distributed sensing technologies are advantageous in that they are minimally invasive and relatively small. In certain industries such as oil and gas, fiber optic sensors have become prevalent because they are able to provide data previously unattainable by conventional sensing techniques that increases yields tremendously [5].

It is clear that fiber optic technology is prevalent and rapidly developing in modern science. As with all new technology, it is vital to identify the challenges faced by these technologies and find solutions to further advance the field. This thesis investigates an interesting phenomena that occurs in side-polished fiber that has the potential to contribute to sensing and telecommunications technology.

Side-polished fiber allows access to the evanescent field propagating in the cladding of the fiber. Access to this evanescent field allows modification of the propagating mode allowing the development of sensing or telecommunication devices. There has been development of

various sensing devices utilizing this access to the evanescent field [6, 7, 8]; however, little has been done to analyze the effect of multimode interaction in side-polished fiber and how specific mode solutions can be employed to create innovative sensing and telecommunication devices. Specifically, allowing the unique interaction of each mode's evanescent field with the side-polished fiber can result vastly different effects for each mode based on the geometry of the fiber. By utilizing mode-specific perturbation, it is feasible to design a mode-domain interferometric sensor. Additionally, such devices could be utilized to create telecommunications devices such as mode multiplexers or optical switches.

Chapter 2

Theory

To help build an understanding of how fiber optics operate, a simple step-index fiber will be introduced and analyzed [9]. Fiber optic operation relies on the principle of total internal reflection (TIR) in a dielectric waveguide structure. Step-index fiber has a simple index profile and is used widely in optical communication and sensing applications. A step-index fiber consists of a core and cladding region with separate indices of refraction. Figure 2.1 shows the cross section and a general refractive index profile for a step-index fiber with a core radius of a and core and cladding indices of n_{co} and n_{cl} respectively. In general, the core index needs to be slightly larger than the cladding index to guide light.

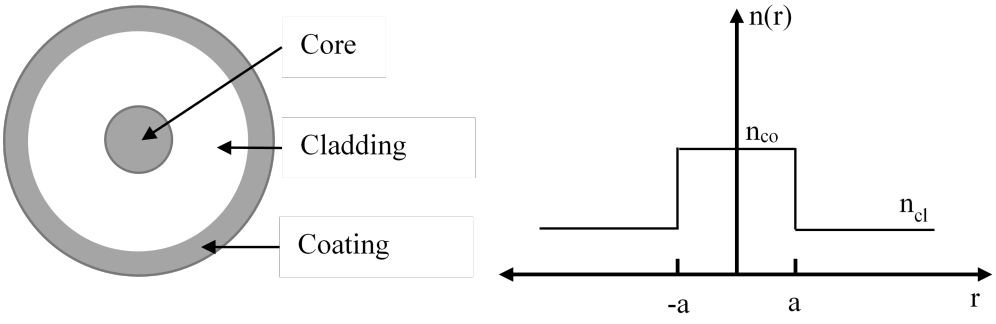

Figure 2.1: Cross section and index profile of a step-index fiber

The guiding of light in the core results from TIR at the core-cladding interface. Figure 2.2 shows a simplistic example of the guided light in a step-index fiber. In reality, light does not travel in a two-dimensional plane, but rather interacts with the surface of the cylindrical fiber

in a more complex manner, but the two-dimensional example presents an easier visualization of the concepts of fiber operation. Using Snell's Law, the smallest incident angle that can occur where light is contained in the waveguide by TIR can be determined. This is defined as the critical angle θ_c.

$$\theta_c = \arcsin\left(n_{cl}/n_{co}\right) \tag{2.1}$$

The maximum angle of acceptance where light is guided in the fiber (θ_i) can then be defined according to equation 2.2.

$$\theta_i = \arcsin\left(n_{co}^2 - n_{cl}^2\right)^{1/2} \tag{2.2}$$

Often, the characteristic used to define the angle of acceptance of a fiber is the numerical aperature (NA).

$$NA = \sin\theta_i = \left(n_{co}^2 - n_{cl}^2\right)^{1/2} \tag{2.3}$$

Another important parameter in fiber optics is the V-number, which is also called the

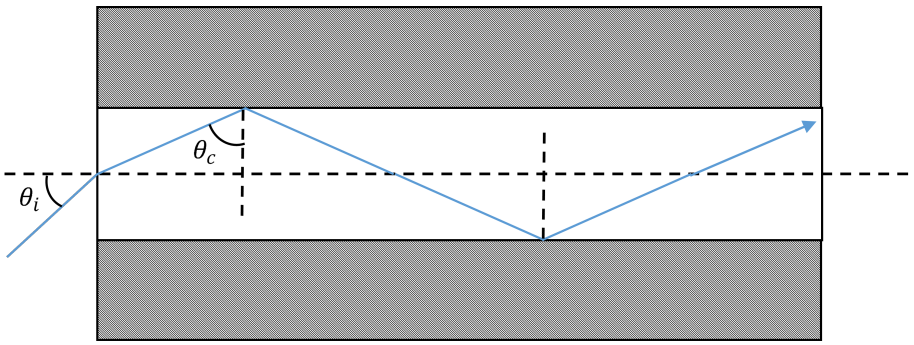

Figure 2.2: A simplified, two-dimensional representation of TIR in a step index fiber

normalized frequency and is defined is defined in equation 2.4. The V-number quantifies the fiber's ability to support transverse modes. The number of modes supported by a fiber increases with V.

$$V = ak(n_{co}^2 - n_{cl}^2)^{1/2} = akNA \tag{2.4}$$

where k is the wavenumber in vacuum $k = 2\pi/\lambda$ and λ is the wavelength of the incident beam. An approximation of the total number of modes supported by a multi-mode step-index fiber is given by $N \approx V^2/2$. The fiber's ability to support multiple modes is vital to the operation of a few-mode device. Commercial fiber is typically advertised to support a specific number of modes at a certain wavelength. The geometry of the fiber is set, but the propagating wavelength can be adjusted to determine the number of modes in the fiber.

2.1 Modal analysis

An optical fiber is a dielectric waveguide that is designed to transmit an electromagnetic field along a specific direction. A fiber mode refers to an electromagnetic field distribution that does not change as it travels along the direction of propagation. Solutions for these equations can be found by solving the wave equations derived from Maxwell's equations and applying boundary conditions representative of the waveguide [9]. There are three classifications of modes: guided modes, leaky modes, and radiation modes. This thesis will only focus on guided modes as optical fibers are designed to transmit guided modes.

2.1.1 Mode solutions in few-mode fiber

Fiber modes are a specific solution of the wave equation that satisfies the boundary conditions of the fiber. A fiber mode has a distinct spatial distribution that does not change when propagating longitudinally assuming the index of refraction remains constant. The first step in analyzing fiber modes is to define the time-harmonic electric and magnetic fields in the

cylindrical coordinate system.

$$\begin{aligned}\mathbf{E} &= \mathbf{E_0}(\rho,\phi)e^{i\omega t}e^{-i\beta z}\\ \mathbf{H} &= \mathbf{H_0}(\rho,\phi)e^{i\omega t}e^{-i\beta z}\end{aligned} \tag{2.5}$$

The three components of each field can be separated into the transverse plane and the propagation direction.

$$\begin{aligned}\mathbf{E} &= \mathbf{E_t} + E_z\mathbf{e_z}\\ \mathbf{H} &= \mathbf{H_t} + H_z\mathbf{h_z}\end{aligned} \tag{2.6}$$

In the cylindrical coordinate system, z is the direction of propagation, ρ is the radial distance from center, and ϕ is the angle relative to the x-axis in the rectangular coordinate system. The geometry of a typical step-index fiber is shown in Figure 2.1. The vector operators for the cylindrical coordinate system are as follows:

$$\begin{aligned}\nabla f &= \mathbf{e}_\rho\frac{\partial f}{\partial \rho} + \mathbf{e}_\phi\frac{1}{\rho}\frac{\partial f}{\partial \phi} + \mathbf{e_z}\frac{\partial f}{\partial z}\\ \nabla^2 f &= \frac{1}{\rho}\frac{\partial}{\partial \rho}\left(\rho\frac{\partial f}{\partial \rho}\right) + \frac{1}{\rho^2}\frac{\partial^2 f}{\partial \phi^2} + \frac{\partial^2 f}{\partial z^2}\\ \nabla\cdot\mathbf{A} &= \frac{1}{\rho}\frac{\partial}{\partial \rho}(\rho A_\rho) + \frac{1}{\rho}\frac{\partial A_\phi}{\partial \phi} + \frac{\partial A_z}{\partial z}\\ \nabla\times\mathbf{A} &= \mathbf{e}_\rho\left[\frac{1}{\rho}\frac{\partial A_z}{\partial \phi} - \frac{\partial A_\phi}{\partial z}\right] + \mathbf{e}_\phi\left[\frac{\partial A_\rho}{\partial z} - \frac{\partial A_z}{\partial \rho}\right] + \mathbf{e_z}\frac{1}{\rho}\left[\frac{\partial}{\partial \rho}(\rho A_\phi) - \frac{\partial A_\rho}{\partial \phi}\right]\end{aligned} \tag{2.7}$$

Equations for the transverse field components are derived from the source-free Maxwell's

equations to perform modal analysis.

$$\begin{aligned} \nabla \times \mathbf{E} &= -i\omega\mu\mathbf{H} \\ \nabla \times \mathbf{H} &= i\omega\varepsilon\mathbf{E} \\ \nabla \cdot \mathbf{E} &= 0 \\ \nabla \cdot \mathbf{H} &= 0 \end{aligned} \tag{2.8}$$

Using the equations in 2.6 and 2.8, it is possible to find a solution the transverse components $\mathbf{H_t}$ and $\mathbf{E_t}$ in terms of the longitudinal components E_z and H_z.

$$\begin{aligned} \mathbf{E_t} &= \frac{-i}{\omega^2\varepsilon\mu - \beta^2}[\beta\nabla_t E_z - \omega\mu\mathbf{e_z} \times (\nabla_t H_z)] \\ \mathbf{H_t} &= \frac{-i}{\omega^2\varepsilon\mu - \beta^2}[\beta\nabla_t H_z + \omega\mu\mathbf{h_z} \times (\nabla_t E_z)] \end{aligned} \tag{2.9}$$

The is significant because it allows solving for the transverse components with the knowledge of only three parameters: the propagation constant β, the longitudinal electric field E_z, and the longitudinal magnetic field H_z.

Assuming the medium is homogeneous, the well known Helmholtz equations can be used to solve for each of these required parameters.

$$\begin{aligned} \nabla_t^2 E_z + k_t^2 E_z &= 0 \\ \nabla_t^2 H_z + k_t^2 H_z &= 0 \end{aligned} \tag{2.10}$$

where $k_t^2 = \omega^2\varepsilon\mu - \beta^2$.

Substituting E_z and H_z into equations 2.9 using the cylindrical vector equations yields

$$\begin{aligned} \frac{1}{\rho}\frac{\partial}{\partial\rho}\left(\rho\frac{\partial E_z}{\partial\rho}\right)+\frac{1}{\rho^2}\frac{\partial^2 E_z}{\partial\phi^2}+k_t^2E_z=0 \\ \frac{1}{\rho}\frac{\partial}{\partial\rho}\left(\rho\frac{\partial H_z}{\partial\rho}\right)+\frac{1}{\rho^2}\frac{\partial^2 H_z}{\partial\phi^2}+k_t^2H_z=0 \end{aligned} \tag{2.11}$$

Separation of variable analysis yields a Bessel equation where F is either E_z or H_z and $l=0,1,2....$

$$\frac{d^2f}{d\rho^2}+\frac{1}{\rho}\frac{df}{d\rho}+\left(k_t^2-\frac{l^2}{\rho^2}\right)f=0 \tag{2.12}$$

By definition, any function that satisfies the Bessel equation can be written as a linear superposition of two solutions (i.e. the Bessel functions of the first and second kind). For the core, h is defined as $h^2=n_{co}^2\frac{\omega^2}{c^2}-\beta^2$ yielding:

$$F(\rho,\phi)=\left[c_1J_l(h\rho)+c_2Y_l(h\rho)\right]e^{il\phi} \tag{2.13}$$

A similar result can be formulated for the cladding by a linear combination of the modified Bessel functions and defining $q^2=\beta^2-n_{cl}^2\frac{\omega^2}{c^2}$

$$F(\rho,\phi)=\left[c_3I_l(q\rho)+c_4K_l(q\rho)\right]e^{il\phi} \tag{2.14}$$

For a fiber optic waveguide the three boundary conditions are: (1) The field is finite and must go to zero as $\rho\to\infty$. (2) The electromagnetic field must remain finite at $\rho\to0$. (3) The transverse field components (E_ρ, E_ϕ, H_ρ, H_ϕ) must be continuous at $\rho=a$. Applying the boundary conditions that the field must be finite in both the core and cladding and that

the field approaches zero as $r \to \infty$ in the cladding, equation 2.13 and equation 2.14 become

$$\begin{aligned} F(\rho,\phi) &= c_1 J_l(h\rho)e^{il\phi} \\ F(\rho,\phi) &= c_4 K_l(q\rho)e^{il\phi} \end{aligned} \tag{2.15}$$

Substituting E_z and H_z into equation 2.15 yields the following solutions for the transverse fields in the core and cladding:

$$\begin{aligned} Core: E_z(\rho,\phi) &= AJ_l(h\rho)e^{il\phi}e^{i\omega t}e^{-i\beta z} \\ H_z(\rho,\phi) &= BJ_l(h\rho)e^{il\phi}e^{i\omega t}e^{-i\beta z} \end{aligned} \tag{2.16}$$

$$\begin{aligned} Clad: E_z(\rho,\phi) &= CK_l(q\rho)e^{il\phi}e^{i\omega t}e^{-i\beta z} \\ H_z(\rho,\phi) &= DK_l(q\rho)e^{il\phi}e^{i\omega t}e^{-i\beta z} \end{aligned} \tag{2.17}$$

Equation 2.16 and equation 2.17 refer to the longitudinal fields propagating in the core and cladding. By substituting these equations into equation 2.9, we now have the information required to solve for the transverse components of the electromagnetic field.

In the core, E_ϕ and H_ϕ can be determined according to equation 2.9

$$\begin{aligned} Core: E_\phi &= \frac{-i\beta}{h^2}\left[\frac{1}{\rho}\frac{\partial E_z}{\partial\phi} - \frac{\omega\mu}{\beta}\frac{\partial H_z}{\partial\rho}\right] = \frac{-i\beta}{h^2}\left[\frac{il}{\rho}AJ_l(h\rho) - \frac{\omega\mu}{\beta}BhJ_l'(h\rho)\right]e^{il\phi}e^{i\omega t}e^{-i\beta z} \\ H_\phi &= \frac{-i\beta}{h^2}\left[\frac{1}{\rho}\frac{\partial H_z}{\partial\phi} + \frac{\omega\varepsilon}{\beta}\frac{\partial E_z}{\partial\rho}\right] = \frac{-i\beta}{h^2}\left[\frac{il}{\rho}BJ_l(h\rho) + \frac{\omega\varepsilon_{co}}{\beta}AhJ_l'(h\rho)\right]e^{il\phi}e^{i\omega t}e^{-i\beta z} \end{aligned} \tag{2.18}$$

The same process can be applied to E_ϕ and H_ϕ in the cladding to obtain

$$\begin{aligned} Clad: E_\phi &= \frac{-i\beta}{h^2}\left[\frac{1}{\rho}\frac{\partial E_z}{\partial \phi} - \frac{\omega\mu}{\beta}\frac{\partial H_z}{\partial \rho}\right] = \frac{i\beta}{q^2}\left[\frac{il}{\rho}CK_l(q\rho) - \frac{\omega\mu}{\beta}DqK_l'(q\rho)\right]e^{il\phi}e^{i\omega t}e^{-i\beta z} \\ H_\phi &= \frac{-i\beta}{h^2}\left[\frac{1}{\rho}\frac{\partial H_z}{\partial \phi} + \frac{\omega\varepsilon}{\beta}\frac{\partial E_z}{\partial \rho}\right] = \frac{i\beta}{q^2}\left[\frac{il}{\rho}DK_l(q\rho) + \frac{\omega\varepsilon_{cl}}{\beta}CqK_l'(q\rho)\right]e^{il\phi}e^{i\omega t}e^{-i\beta z} \end{aligned} \tag{2.19}$$

Applying the previously defined boundary conditions to the equations above (i.e. 2.16, 2.17, 2.18, 2.19) a matrix can be formulated to solve for the remaining unknows of the mode solutions.

$$\begin{bmatrix} J_l(ha) & 0 & -K_l(qa) & 0 \\ 0 & J_l(ha) & 0 & -K_l(qa) \\ \frac{il}{h^2a}J_l(ha) & -\frac{\omega\mu}{h\beta}J_l'(ha) & \frac{il}{q^2a}K_l(qa) & -\frac{\omega\mu}{q\beta}K_l'(qa) \\ \frac{\omega\varepsilon_{co}}{h\beta}J_l'(ha) & \frac{il}{h^2a}J_l(ha) & \frac{\omega\varepsilon_{cl}}{q\beta}K_l'(qa) & \frac{il}{q^2a}K_l(qa) \end{bmatrix} \begin{bmatrix} A \\ B \\ C \\ D \end{bmatrix} = 0 \tag{2.20}$$

Solving the above matrix will determine the values of β and the coefficients A, B, C and D giving us a discrete solution to both the transverse and longitudinal components of the electromagnetic fields. However, the solving for these coefficients is computationally intensive and time consuming. Instead, an approximation can be made under the weakly-guided regime when $n_{co} \approx n_{cl}$ which will significantly decrease the computational intensity.

2.1.2 Mode solutions in the weakly-guiding regime

The vast majority of optical fibers are weakly-guiding, which means that the refractive indices of the core and cladding are very close to each other ($n_{co} \approx n_{cl}$). The main reason for optical fibers having such a small refractive index change is because of fabrication. The core

and cladding are typically made of the same material and dopants are used to create the refractive index profile. A high concentration of dopants is generally unsuitable since it can cause unwanted effects such as nonlinearity; therefore, most fibers have a relatively small $\Delta = n_{cl} - n_{co}$ with an order of magnitude around 10^{-3}. Theoretically, the weakly-guided regime allows significant simplification of the mode solution.

Under the weakly-guiding approximations, the transverse fields of the fiber modes are assumed to be polarized in one direction (i.e. linearly polarized). The linearly polarized (l, m) modes are denoted as LP_{lm} modes where l is the azimuthal order and m is the radial order. Each LP mode travels with the same propagation constants and spatial distribution.

The characteristic equation for weakly-guiding fibers is approximately equivalent to the conditions of the scalar functions in equation 2.15. Additionally, the transverse field components are continuous at the interface the function $F(\rho, \phi)$ in equation 2.15 and its derivative are continuous at $r = a$. These conditions are satisfied when

$$\frac{(ha)J_{l-1}(ha)}{J_l(ha)} = \frac{(qa)K_{l-1}(qa)}{K_l(qa)} \tag{2.21}$$

The derivatives of Bessel Functions satisfy the identities

$$\begin{aligned} J_l'(x) &= \pm J_{l\mp1}(x) \mp l\frac{J_l(x)}{x} \\ K_l'(x) &= -K_{l\mp1}(x) \mp l\frac{K_l(x)}{x} \end{aligned} \tag{2.22}$$

Substituting these identities into equation 2.21 along with the normalized parameters $X = ha$ and $Y = qa$ yields the characteristic equation

$$\boxed{X\frac{J_{l\pm1}(X)}{J_l(X)} = \pm Y\frac{K_{l\pm1}(Y)}{K_l(Y)}} \tag{2.23}$$

Provided the V-number (equation 2.4) and l are given, the only unknown variable in the above equation is X since $Y^2 = V^2 - X^2$. The equation can be solved graphically by plotting both sides of the equation versus X and observing where they intersect to determine X.

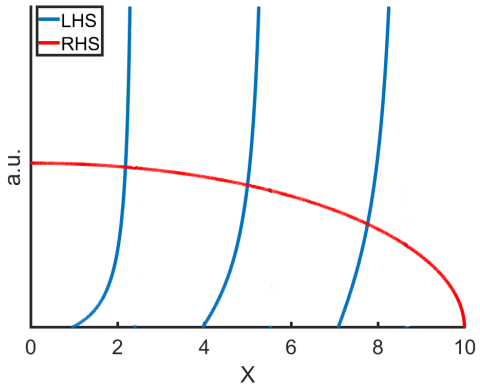

Figure 2.3: Graphical solution to the characteristic equation 2.23
The left-hand side (LHS) and right-hand side (RHS) are plotted as functions of X. The intersections are the solutions to the equation. The total number of intersections indicates the number of modes in the fiber. In this plot, the V-number is 10 and $l = 0$

It is clear from Figure 2.3 that number of modes in the fiber increases with V. In fact, the mode cutoff value of V can be found for any combination of l and m by numerically solving the characteristic equation. These cutoff V values can be found in Table 2.1 for $l = 0, 1$ and $m = 1, 2, 3$.

Table 2.1: Cutoff V parameters for the LP_{lm} modes

m	1	2	3
$l = 0$	0	3.832	7.016
$l = 1$	2.405	5.520	8.654

Each mode has a distinct radial distribution $u(\rho, \phi)$ (equation 2.15).

$$u(\rho) \propto \begin{cases} J_l(h\rho), & \rho \leq a \\ K_l(q\rho), & \rho > a \end{cases} \tag{2.24}$$

Since (l, m) and $(-l, m)$ modes have the same propagation constant, the superposition of these two modes leads to an interesting spatial distribution where the complex amplitude of the sum is proportional to $u_{lm}(\rho)\cos(l\phi)\exp(-i\beta_{lm}z)$. The intensity $I(\rho, \phi)$ is then proportional to

$$I(\rho, \phi) \propto u_{lm}^2(\rho)\cos^2(l\phi) \tag{2.25}$$

The fiber used for the experimental results presented in Chapter 4 is Thorlabs SM980-5.8-125. This particular fiber operating at 660 nm has a V-number of 3.59 indicating that the LP_{01} and LP_{11} modes are supported in the fiber (Table 2.1). The graphical solutions for the characteristic equation are shown for each mode in Figure 2.4.

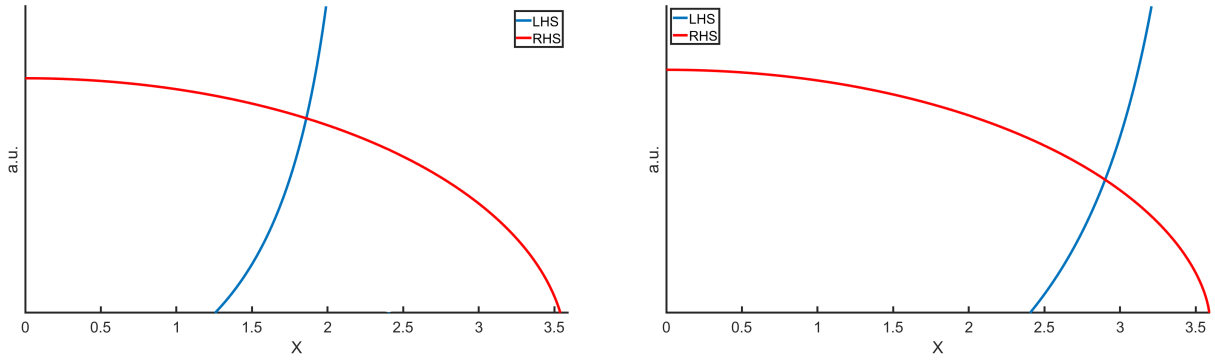

(a) LP_{01} (b) LP_{11}

Figure 2.4: Graphical solution of the characteristic equations for Thorlabs SM980-5.8-125 operating at 660nm ($V = 3.59$). (a) $X_{01} = 1.877$ (b) $X_{11} = 2.901$

Table 2.2 shows the results of the numerical analysis and the values of needed to solve for the intensity distribution of the LP modes. X was determined from the intersection of the left and right hand side of the characteristic equation, while Y was calculated according to the relationship $Y^2 = V^2 - X^2$.

At this point, the LP mode intensity distribution can be determined using the values in Table 2.2 along with equations 2.24 and 2.25. The spatial intensity distribution of each mode is

Table 2.2: LP mode parameters determined by numerical analysis of the characteristic equation (i.e. X, Y, and V)

	V	X	Y
LP_{01}	3.59	1.88	3.06
LP_{11}	3.59	2.90	2.11

presented in Figure 2.5. These distributions will be vital in describing the behavior of each mode when a portion of the cladding is removed. In particular, comparing the number of modes and spatial distributions for LP modes in a standard fiber to the geometry of side-polished fiber provides valuable insight into how the evanescent field in the cladding interacts with the polished surface of the fiber.

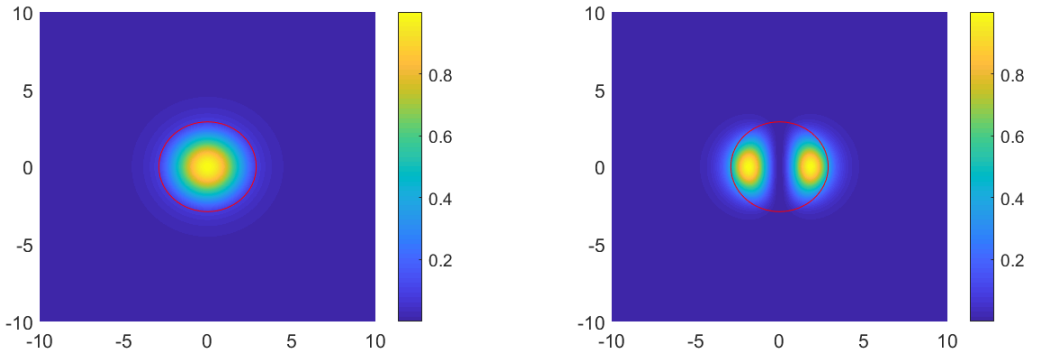

(a) LP_{01} (b) LP_{11}

Figure 2.5: Spacial Distribution of the LP modes' intensity present in Thorlabs SM980 Fiber operating at 660nm. The red circle represents the fiber core ($a = 2.9\mu m$)

2.2 Side-polished fiber

A side-polished fiber (SPF) is a typical optical fiber with a portion of the cladding partially removed to gain access to the guided wave in the fiber. SPF is used in many applications such as directional couplers [10], polarizers [11, 12, 13], modulators, switches [14], amplifiers [15], and filters [16]. Figure 2.6 shows the cross-sectional view of the polished fiber.

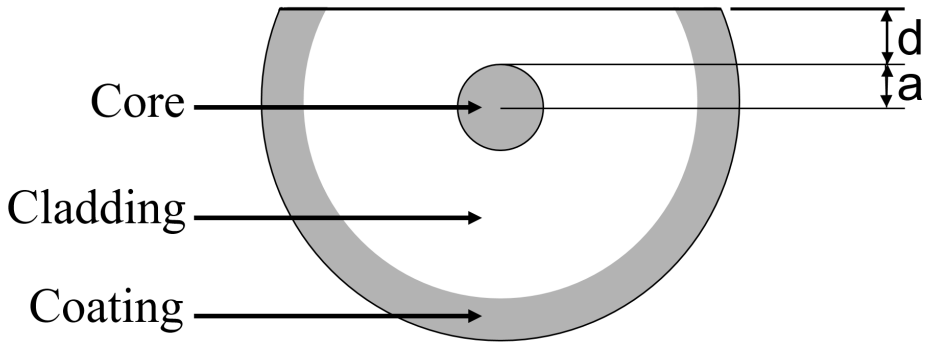

Figure 2.6: Cross-sectional view of a side-polished fiber where a is the core radius and d is the distance from the core to the polished surface.

The profile of the SPF can be compared to the schematic for a step-index fiber shown in Figure 2.1. The SPF geometry provides access to the evanescent field propagating in the cladding of a few-mode fiber. The evanescent field can then be perturbed with a number of different variables, such as a change in refractive index or a reflective surface a specific distance away, to create sensors and optical devices. Most existing research in SPF devices is done with single-mode operation due to the complexity of the mode interactions at the polished surface. However, this research presents an interesting phenomenon where with careful design and fabrication, multi-mode operation can provide unique opportunities for a new class of SPF devices utilizing the interaction of the physical geometry of a side-polished fiber with the spatial distribution of the LP modes.

2.2.1 LP modes in side-polished fiber

Solving for the exact mode solutions in side-polished fiber is fairly complex due to the added boundary at the polished surface and the break in cylindrical symmetry. However, if it is assumed that most of the mode is contained in the core, an approximation can be made where the LP modes of the step-index fiber presented in Section 2.1.2 also propagate in the polished fiber. Depending on how close the polished surface is to the core, some or all of the mode propagating in the cladding portion of the fiber will interact with the polished surface. To confirm this approximation, the LP modes of the step index fiber will be compared to the geometry of a typical polished fiber to determine whether the mode will interact with the polished surface. Additionally, experimental results will confirm the validity of this approximation.

LP modes in side-polished fiber are especially hard to solve for analytically due to the asymmetrical cross-sectional geometry. Instead, the LP modes determined in Section 2.1.2 relating to the few-mode fiber will be compared to the geometry of the SPF in order to visualize the interaction between the LP mode and the polished surface. The most important parameter to define when analyzing a side-polished fiber is the distance between the core and the polished surface.

Referring to Figure 2.7a, it is clear that the LP_{01} mode is symmetric. This indicates that the orientation of polishing does not effect how the mode behaves. However, the LP_{11} mode is asymmetric (Figures 2.7b and 2.7c). More interaction will occur if the polished surface is near the region of higher magnitude in the cladding (LP_{11}^{-}). Because of this asymmetry, it is important to to determine the orientation of the mode with the fiber geometry. In practice, this is done by calibrating a phase-only spatial light modulator in the experimental setup and carefully orienting the side-polished fiber during testing.

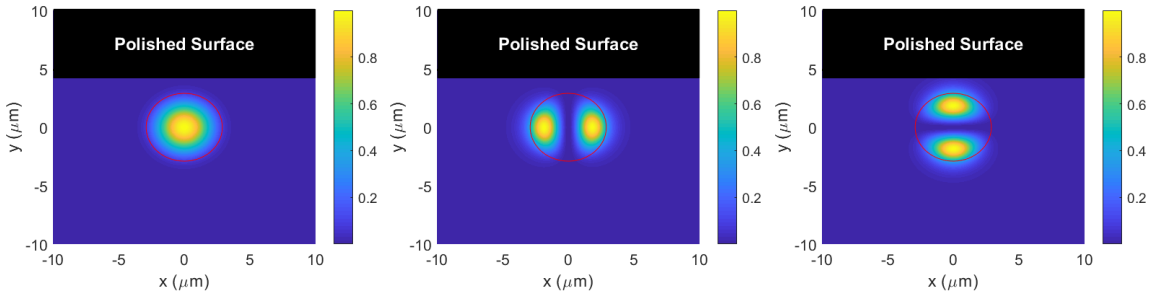

(a) LP_{01} (b) LP_{11}^{+} (c) LP_{11}^{-}

Figure 2.7: LP modes in side-polished fiber

Observing mode interaction with the polished surface will be important in analyzing the experimental results as the mode-dependent loss characteristics demonstrated are explained by mode proximity. When the mode propagating in the core is close to the surface, it has a strong interaction with the polished surface and anything that is located at the surface. If a certain mode has a stronger interaction with the surface than another mode, there will be mode-dependent interactions. This allows the design of mode-domain sensors using interferometry or even telecommunications devices where you can use a side-polished fiber to filter out a specific mode. Changing the material at the surface also will also effect the behavior of the device. If the refractive index is changed, the amount of light that continues to propagate will be effected. Additionally, if a material is placed on the surface that absorbs a specific wavelength of light, a mode propagating at that wavelength will be attenuated when propagating at the polished surface. There are numerous applications that mode-domain SPF devices can be applied to, but first the behavior of such devices must be demonstrated experimentally.

Chapter 3

Methods

Experimentally analyzing the behavior of modes in side-polished fiber (SPF) requires delicate fabrication and careful design of the experimental setup. Optical fiber is too small and fragile to be polished alone, so support is required when fabricating and analyzing the fibers. Silicon wafer is chosen as the support during fabrication and experimentation mainly due to precise groove fabrication by anisotropic etching. A phase-only spatial light modulator (SLM) (Holoeye, Pluto) is used to control the modes propagating through the fiber. Since the fiber chosen for the experiment (Thorlabs SM980-5.8-125) supports two modes at the laser wavelength (660 nm), the SLM is used to analyze each mode individually by only allowing the mode being studied to propagate in the fiber.

The intensity of each mode is measured for two conditions: (1) the polished fiber surface is exposed to air, (2) a solution of gold nanoparticles is on the polished fiber surface. This provides a (1) low-loss and (2) high loss case if the mode is interacting with the polished surface. By analyzing the loss ratio between these two cases, some interesting conclusions can be drawn on how modes propagate through side-polished fiber.

3.1 Fabrication of side-polished fiber

The side-polished fiber is fabricated using diamond lapping (polishing) sheets. The polishing begins with a high grit (15 μm) and gradually decreases in grit size until final polishing grit

(0.5 μm) at the desired polishing depth. The fiber is attached to a silicon wafer with a groove (Figure 3.1) to hold the fiber in place during polishing. The groove in the silicon wafer is fabricated by anisotropic etching. The dimensions of the groove are determined by the fiber that is being etched. For Throlabs SM980-5.8-125, the desired grove dimensions are $w = 128\mu m$ and $h = 67\mu m$. This allows the fiber to fit into the groove with little movement and gave an approximation for the depth of polishing based on the surface of the silicon wafer.

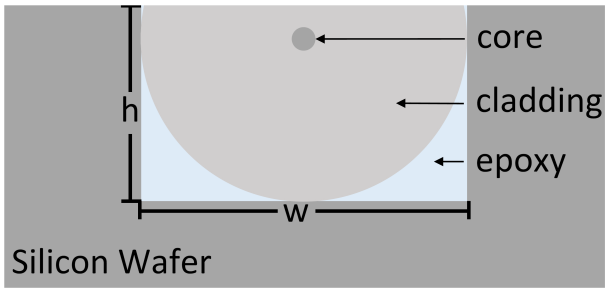

Figure 3.1: Cross-section view of fiber fabrication setup.

The polishing surface is periodically rinsed with Isopropyl Alcohol (IPA) to clean the surface and limit any unwanted abrasions caused by debris left on the surface during polishing. Once the desired depth is reached, the surface is rinsed with IPA and distilled water to remove any residue and debris on the polished surface.

Determining the distance between the polished surface and the core is difficult because a few micron difference in polishing depth creates a significant difference in the behavior of the SPF. The most accurate way to measure the polishing depth is by taking an cross-sectional image of the fiber under a scanning electron microscope (SEM) as shown in Figure 3.2.

Unfortunately, to acquire this image, the fiber must be broken and sputter coated rendering the fiber useless for later optical analysis. Therefore, the fabrication process is calibrated by fabricating numerous SPF of different polishing depths and compared their transmis-

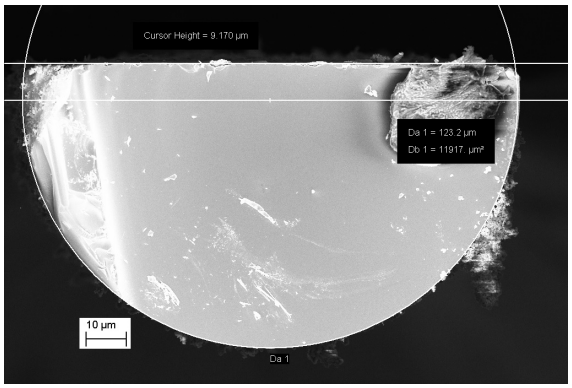

Figure 3.2: SEM image showing the cross section of a SPF where the height $d = 6.27\mu m$. The fiber used in the image is Thorlabs SM980-5.8-125 which has a core diameter of $5.8\mu m$ and a total diameter of $125\mu m$

sion percentage to the polishing depths determined by the SEM images. The transmission percentage T is defined by

$$T = \frac{I_p}{I_u} \times 100\% \tag{3.1}$$

where I_p is the intensity measured at the output of the polished fiber and I_u is the intensity measured at the output of the unpolished fiber. The intensities are measured using a photodetector which is connected to the SPF as shown in Figure 3.3.

Figure 3.3: Experimental setup for determining the transmission percentage (T) based on the output intensities measured by the photodetector (i.e. I_u and I_p)

To complete calibration of the fabrication process, the fiber polishing depth was compared to the transmission value for each fiber. As expected, there was a correlation between polishing depth and the transmission percentage, which can be seen in Table 3.1. Using this method,

SPF can be fabricated to within two micron accuracy.

Table 3.1: Calibration of SPF fabrication.

Distance from core (d)	Transmission (T)
$3\mu m$	$7 \pm 1\%$
$5\mu m$	$10 \pm 1\%$
$7\mu m$	$20 \pm 3\%$
$9\mu m$	$35 \pm 5\%$

3.2 Experimental setup

The experimental setup is shown in Figure 3.4. Light from a linearly polarized laser diode operating at 660.7 nm is passed through a half-wave plate for polarization control. The beam then passes through a lense to expand the wave and subsequently propagates through a linear polarizer to select the waves parallel to the optical table. This polarization direction is the same as the phase modulation axis of the spatial light modulator (SLM). Therefore, the half wave plate can be rotated to obtain maximum power after P1. After the beam passes through P1, it is reflected by a mirror towards the phase-only SLM (Holoeye, Pluto) which reflects the beam again towards P2. The SLM is used to select the desired transmitted mode; LP01 or LP11. Feedback from the CCD to the computer is used to calibrate the SLM to produce the desired mode profile. P2 is used to ensure only a single polarization component of the optical output is monitored. The beam is then focused into the fiber (Thorlabs SM980-5.8-125) using an objective lens (L1, 20x).

The polished portion of the fiber is designed with one side of the cladding being polished to a depth of 3-10 μm from the fiber core with a propagation length in the polished section of 3 cm. Modes propagating down this portion of the fiber will interact with any material on the surface of the fiber. After the light propagates through the fiber, the light passes

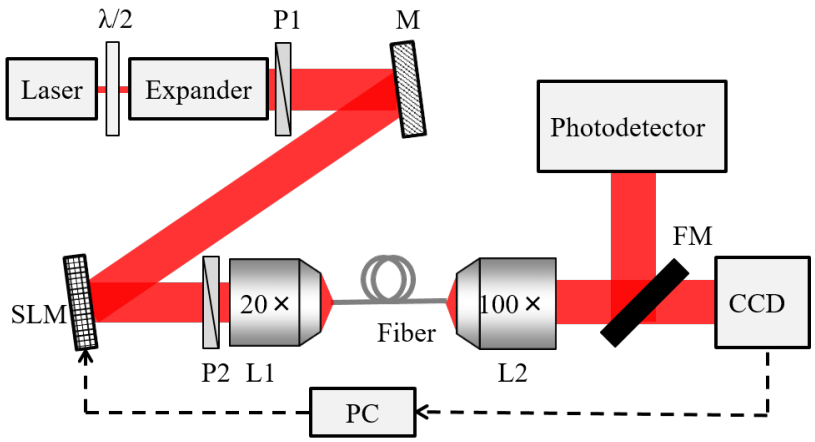

Figure 3.4: Experimental setup

through an objective lens (L2, 100x) and is finally split by a beam splitter (BS) where the light is collected by a photodetector (PD) and a CCD camera. The CCD camera is primarily used to calibrate the SLM so the proper beam is injected into the fiber for sensing. The PD measures the output intensity of the light.

3.2.1 Spatial light modulator calibration

The adaptive control of the mode profile at the output of the fiber is based on image analysis with the CCD camera. To calibrate the desired mode, a normalized correlation function is defined as

$$F = \frac{\iint I_{CCD}(x,y) I_t(x,y) dxdy}{\sqrt{\iint I_{CCD}^2(x,y) dxdy} \sqrt{\iint I_t^2(x,y) dxdy}} \tag{3.2}$$

where $I_{CCD}(x,y)$ represents the optical intensity distribution at the fiber output and $I_t(x,y)$ is the spatial profile of the target profile. It is clear that the equation represents the similarity between the CCD camera image and the target profile. When the CCD image perfectly

matches the target, F becomes unity. The procedure for adaptive mode control uses a step-wise sequential algorithm where the SLM is divided into 13x13 equal sized phase blocks where each block can produce a reflection phase in the range of $[0, 2\pi]$. The feedback signal is then measured and the new wavefront is either accepted or rejected based on whether F is closer or further from unity. Using this process, the optimized mode profile is determined where F is closest to unity.

3.2.2 Mode optimization

Mode optimization in a standard, unpolished single-mode fiber is shown in Figure 3.5a. The process of achieving unity normalized correlation function as defined in equation 3.2 was employed to determine the optimized LP_{01}, LP_{11}^{+}, and LP_{11}^{-} modes in the SM980 fiber. The optimized wavefront indicates the best optimization realized by the SLM using the setup and method outlined above.

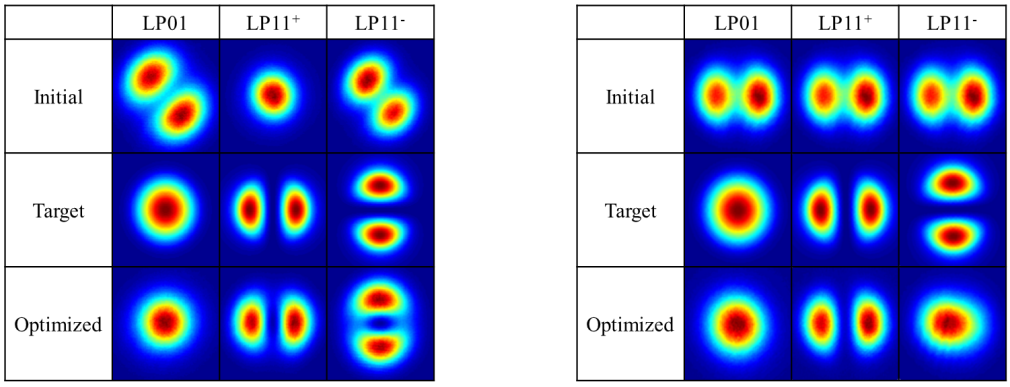

(a) Standard fiber (b) Side-polished fiber

Figure 3.5: Comparison between the mode calibration of a standard fiber (a) and a SPF (b). Notice the difference between the LP_{11}^{-} optimized modes.

Calibration of the mode profile was also performed on samples of varying side-polished depths to determine the mode responses. Figure 3.5b shows the optimization process for a sample polished to 5 μm from the core. It is clear that only one orientation of the LP11 mode

is realized in the SPF. Unlike the unpolished fiber optimization shown in Figure 3.5a, the polished fiber optimization failed for the LP_{11}^{-} mode. An explanation to why the LP_{11}^{-} mode cannot be realized by SLM optimization is due to the geometry of the SPF.

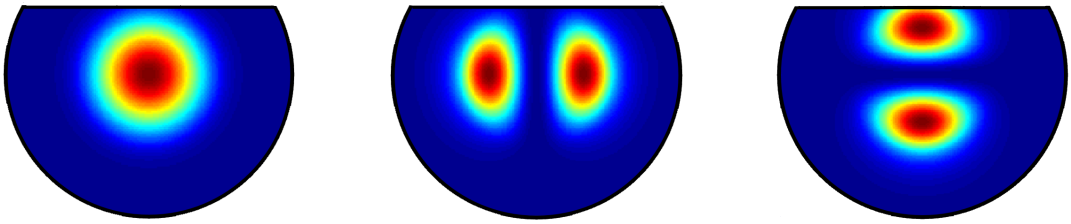

(a) LP_{01} (b) LP_{11}^{+} (c) LP_{11}^{-}

Figure 3.6: SPF geometry comparison to the target modes for the SLM. The LP_{11}^{-} mode (c) can not be optimized using the SLM.

Figure 3.6 shows how the each mode aligns with the polished fiber cross-section. The LP_{11}^{+} orientation is contained within the unpolished fiber and is able to be optimized by the SLM. However, much of the LP_{11}^{-} mode propagates at the polished portion of the fiber, which means that the light interacts strongly with the polished surface. This results in the LP_{11}^{+} orientation being able to propagate through the SPF, while the LP_{11}^{-} orientation is not able to reach a suitable correlation factor (i.e. $F \neq 1$) and is unable to propagate.

3.3 Loss conditions

It has been established that any perturbation to the polished surface of the side-polished fiber should effect the evanescent field propagating in the cladding. To verify this claim, an gold nanoparticle solution (GNS) is placed on the polished surface to absorb a portion of the evanescent field (Figure 3.7). Gold nanaoparticles exhibit strong optical absorbtion and scattering across the visible to near infrared spectrum. Since the operating wavelength chosen is 660nm, light propagating near the GNS will be absorbed. Each mode has a

different percentage of light propagating near the polished surface. This can be confirmed by allowing each mode to propagate in the fiber independently and measuring the amount of light absorbed by the gold nanoparticle solution.

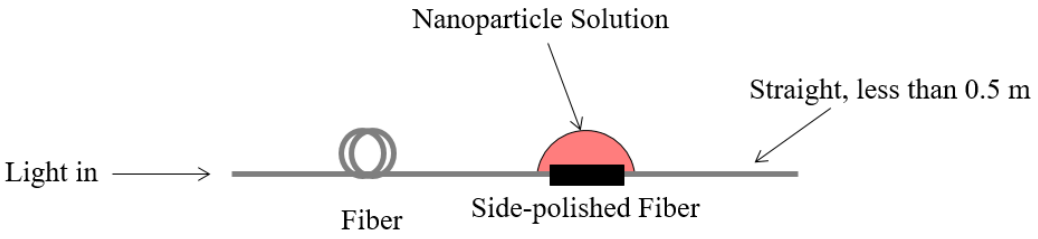

Figure 3.7: Side-polished fiber with a droplet of gold nanoparticle solution on the polished surface

The method for determining loss from the gold nanoparticles on the surface is to measure the output intensity when there is no solution on the polished surface to establish an initial intensity and measure the output intensity after the solution is on the polished portion to determine final intensity. This will establish a loss percentage L_{lm} defined by

$$L_{lm} = \frac{I_i - I_f}{I_i} \times 100\% \tag{3.3}$$

where I_i refers to the initial intensity and I_f refers to the final intensity. l and m are used to denote the mode number.

To determine the the influence of the GNS on loss for each mode, a loss ratio is introduced to compare two modes exposed to identical perturbations. If one of the modes has a greater loss ratio, it can be determined that more of that mode is absorbed by the gold nanoparticle solution. This ratio is defined as

$$R = \frac{L_{01}}{L_{11}} \tag{3.4}$$

Therefore, the loss ratio R will indicate whether one of the three following loss conditions:

(1) if $L_{lm} \approx 0$ for all values of n then there is no loss due to the gold nanoparticle solution being deposited on the surface.

(2) if $L_{lm} > 0$ and $R = 1$ there is loss, but it is not mode-dependent. Both modes are experiencing an equal amount of loss due to the GNS being deposited on the polished fiber.

(3) if $L_{lm} > 0$ and $R \neq 1$ there is mode-dependent loss. In this case, one of the modes is experiencing more loss than the other when the GNS is deposited on the polished fiber

Case (3) is where some interesting conclusions can be drawn. Since the only variable being changed between each test is the mode, the mode with more loss must propagate closer to the polished surface. Specifically, if $R > 1$ the LP_{01} mode propagates closer to the surface of the fiber and any perturbation to that surface will effect the LP_{01} mode more. Likewise, if $R < 1$ the LP_{11} mode propagates closer to the polished surface and any perturbation to that surface will effect the LP_{11} mode more. Either conclusion drawn from case (3) will promote the development of mode-based fiber optic devices such as interferometric sensors since each mode can be manipulated individually based on the geometry of the fiber and the perturbation at the surface of the fiber.

Chapter 4

Experimental Results

The results presented focus primarily on determining mode-dependent loss in the side-polished fiber (SPF) to show that the LP_{01} and LP_{11} modes can be distinguished based on the loss at the fiber output. It is also noteworthy to determine the fiber parameters necessary to achieve mode-dependent loss as not all side-polished fibers experience the same effects when a purturbation is applied to the polished surface. In fact, all three of the possible conclusions outlined in Section 3.3 can be achieved just by changing the polishing depth by a few micron.

4.1 No loss condition

The no loss condition occurs when the distance from the polished surface to the core is relatively large (i.e. $d > 9\mu m$). This corresponds to a fabrication transmission greater than 35 percent according to Table 3.1. Figure 4.1 shows an example of the transmission of the LP_{01} and LP_{11} modes before and after the gold nanoparticle solution was deposited on the polished surface of the fiber.

Using equation 3.3, the loss percentage for both LP_{01} and LP_{11} is approximately 0% since the mean output intensity remains the same before and after the gold nanoparticle solution is placed on the polished fiber.

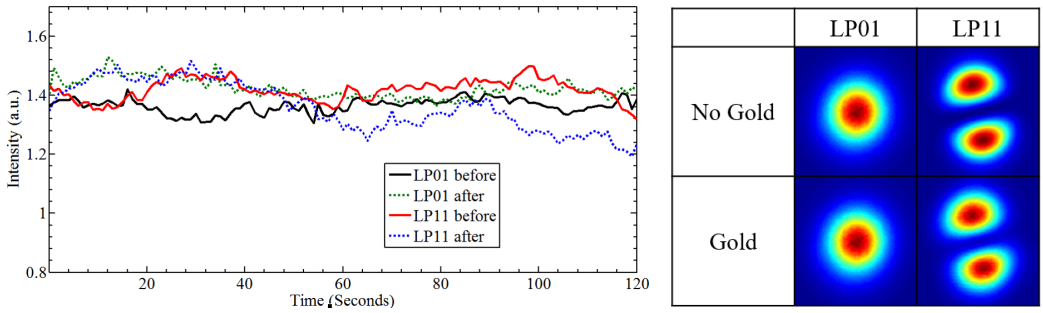

(a) (b)

Figure 4.1: (a) Output intensities and (b) CCD camera image of the mode profile at fiber output for the no loss condition

Since no loss occurs from a polishing depth of approximately 9µm from the core, it is safe to assume that the LP01 and LP11 modes propagate with minimal interaction with the polished surface. Thus, none of intensity of either mode is lost through absorption by the gold nanoparticle solution at the polished surface. In this case, neither mode's evanescent field is propagating close enough to the surface of the fiber to experience an effect of the GNS.

4.2 Mode-independent loss

The conditions for mode-independent loss occur when the distance between the polished surface and the core is relatively small (i.e. $d \approx 3\mu m$). This corresponds to a fabrication transmission of around 7 percent according to Table 3.1. Figure 4.2a shows an example of the transmitted intensities of the LP_{01} and LP_{11} modes before and after the gold nanoparticle solution was deposited on the polished surface of the fiber. Figure 4.2b shows the CCD image of the mode profiles before and after the GNP was deposited on the polished fiber.

Table 4.1 shows the loss percentages and the loss ratio for a few polishing depths that resulted in no mode-dependent loss. The loss ratio R varies from 0.97 to 1.3 indicating that the loss

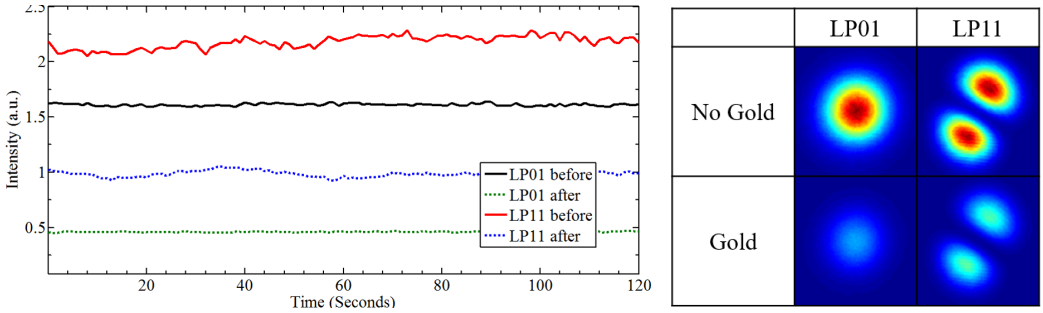

(a) (b)

Figure 4.2: (a) Output intensities and (b) CCD camera image of the mode profile at the fiber output for the mode-independent loss condition

percentage for LP_{01} and LP_{11} modes are relatively similar (i.e. $L_{01} \approx L_{11}$).

Table 4.1: Mode-independent loss

Transmission	L_{01}	L_{11}	R
5%	71.5%	54.9%	1.3
6%	59.3%	52.3%	1.1
7%	20.3%	19.6%	1.0
8%	21.0%	24.5%	0.97

When the polishing depth is close enough to the core, both modes experience significant loss because they are propagating near or at the polished surface allowing light to be absorbed by the gold nanoparticle solution. This is considered mode-independent because the loss ratio is approximately one, indicating the modes experience roughly the same loss percentage. Here the perturbation has a significant effect on the mode intensities, but nothing can be determined from the ratio between the two because they are both experiencing significant loss.

4.3 Mode-dependent loss

Mode-dependent loss is the condition of most interest when designing sensors or devices with a side-polished fiber utilizing the differences in mode interaction. The conditions for mode-dependent loss occur when the distance between the polished surface and the core is approximately $5\mu m$ from the core (i.e. $d = 5\mu m$). This corresponds to approximately 10 percent transmission during fabrication according to Table 3.1. Figure 4.3a shows an example of the transmitted intensities of the LP_{01} and LP_{11} modes before and after the gold nanoparticle solution was deposited on the polished surface of the fiber. Figure 4.3b shows the CCD image of the mode profiles before and after the GNP was deposited on the polished fiber. Table 4.2 shows the loss percentage of polished fibers near 10% transmission.

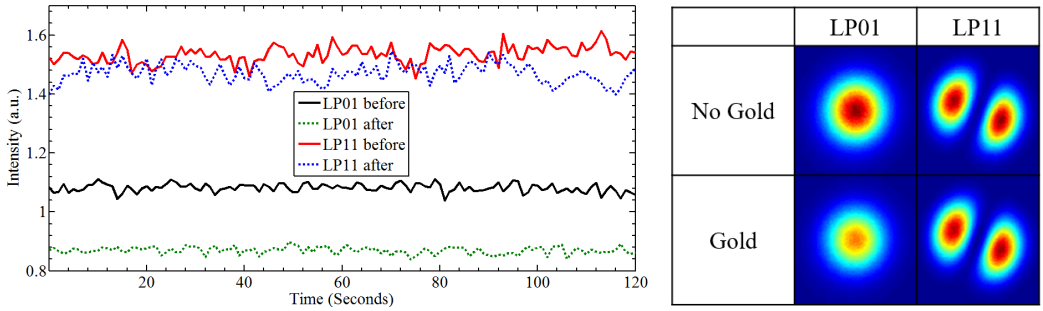

(a) (b)

Figure 4.3: (a) Output intensities and (b) CCD camera image of the mode profile at the fiber output for the mode-dependent loss condition

Comparing these results to the no mode-dependent loss results in Table 4.1 it is clear that the loss ratio (R) is much higher for a polishing depth closer to $5\mu m$. This indicates that more of the LP_{01} mode is being absorbed by the gold nanoparticle solution on the surface. This results in a significant portion of the mode being absorbed by the gold nanoparticle solution and the intensity is not reaching the output of the fiber.

When the loss ratio is not one, it can be concluded that the perturbations on the polished

surface are having a greater effect on one of the modes. Utilizing this ratio, it is possible to design a device that senses other perturbations (temperature, pressure, etc) based on the difference in loss between the modes. Anything that can change how light propagates at the surface of the fiber will effect this ratio because there is a more significant interaction with one of the modes at the surface. The significance of these results will be discussed in more depth in Chapter 5.

Table 4.2: Mode-dependent loss

Transmission	L_{01}	L_{11}	R
9%	32.2%	11.5%	2.8
10%	19.6%	4.2%	4.7
11%	15.3%	3.5%	4.4

4.4 Summary of Results

The modes in the side-polished fiber react differently depending on the distance between the polished surface and the core. When the distance is relatively large (i.e. $d > 9\mu m$, the modes experience no loss when the gold nanoparticle solution is deposited on the surface (Section 4.1). This is because the evanescent field in the cladding is not propagating close enough to the polished surface to interact with the gold nanoparticle solution.

When the fiber is polished to the point where the polished surface is very close to the core, both modes experience significant loss when the gold nanoparticle solution is deposited on the surface of the fiber (i.e. $d \approx 3\mu m$). This occurs because the the evanescent field of both modes is propagating at or near the polished surface resulting in a strong interaction between the propagating mode and the material on the polished surface. When both modes are propagating near the polished surface, it is much harder to distinguish which core has a

stronger interaction which makes this case unsuitable for sensor design.

Finally, the most interesting result occurs when the distance between the core and polished surface is approximately $5\mu m$. At this distance, the LP_{01} mode in the cladding interacts more with the material at the polished surface than the LP_{11} mode. This results in the LP_{01} mode experiencing a greater loss percentage when the gold nanoparticle solution is deposited on the polished surface. This result is of significance because it provides the framework for designing mode-domain sensors and devices with side-polished fibers.

To further analyze the results, the mode profiles determined in Section 2.1.2 will be compared to the polishing depths in each case in Chapter 5. This will provide insight to whether the experimental results match expectations determined by the LP mode solutions.

Chapter 5

Discussion

To help understand the behavior of the side-polished fiber (SPF) presented in Section 4, it is worthwhile comparing the results to the expected behavior of the SPF. One way to determine the expected loss is to look at the spatial distribution of the LP_{01} and LP_{11} modes in a step-index fiber and compare them to the geometry of the SPF. It was previously noted in Section 3.2.2 that only one orientation of the LP_{11} mode propagates in the SPF due to the geometry. Therefore, it is clear that the mode propagation is greatly effected by the geometry of the SPF and it is valuable analyzing the spatial distributions of each mode. Solving for the mode profile according to Section 2.1.2 gives an idea of how each mode will propagate depending on the depth of polishing.

The case most relevant to sensing applications is when one of the modes experiences more loss than the other when the polished surface is modified (i.e. mode-dependent loss). This condition occurred when the polishing depth was approximately $5\mu m$.

Figures 5.1a and 5.1b depict the LP_{01} and LP_{11} modes with the side-polished fiber geometry shown for the case where $d = 5\mu m$. The angle ϕ is given by the equation

$$\phi = \arctan \frac{x}{(d+a)} \tag{5.1}$$

where d is the distance from the polished surface to the core and a is the core radius (see Figure 2.6). x is an arbitrary width of interaction at the surface of the polished fiber. By

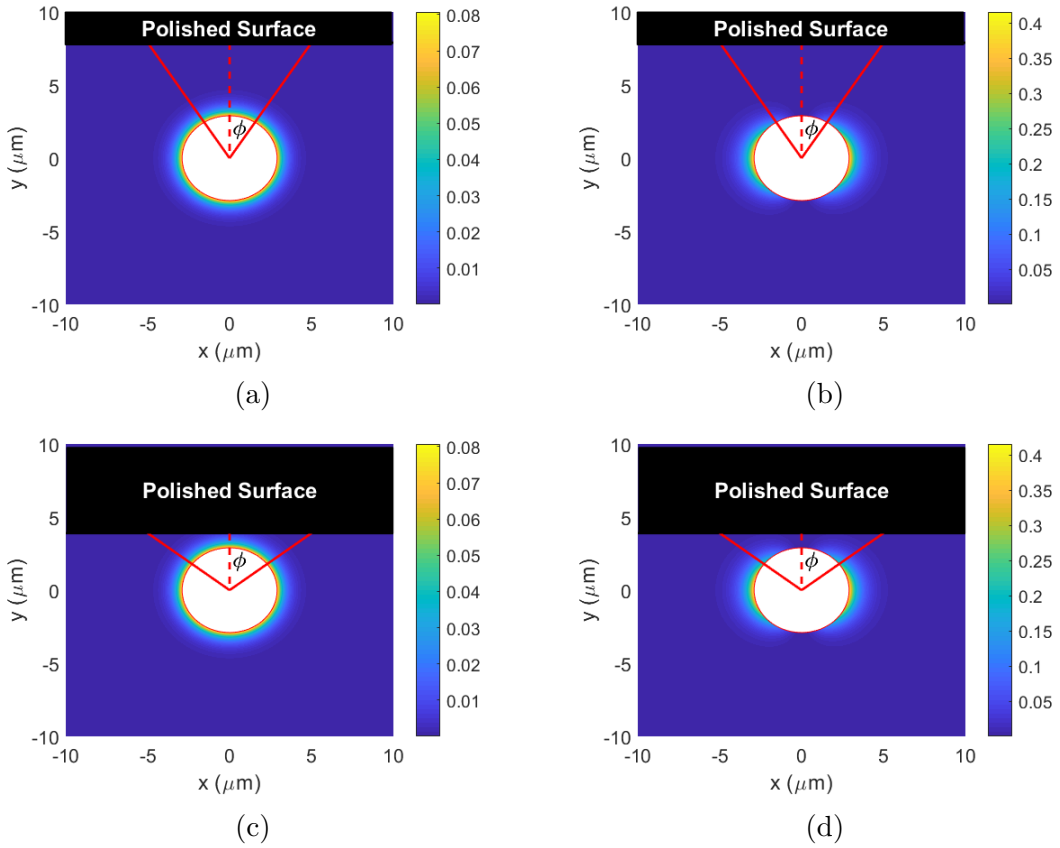

Figure 5.1: (a) LP_{01} and (b) LP_{11} modes for the mode-dependent case ($d = 5\mu m$). (c) LP_{01} and (d) LP_{11} modes for the mode-independent case ($d = 1\mu m$).

creating a wedge indicating the portion of the mode that interacts with the surface of the polished fiber, it is possible to approximate how much of the mode will be effected by a change at the surface of the side-polished fiber.

It is reasonable to determine visually that a larger percentage of the cladding mode is present in the wedge for the LP_{01} mode since most of the LP_{11} mode is concentrated around the region near $\phi = \pi/2$. This result is consistent with the experimental results for the mode-dependent loss case where it was determined that a greater percentage of the LP_{01} mode was lost when the gold nanoparticle solution was deposited on the polished surface.

The result where mode-dependent loss is seen only occurs when there is a balance between being close enough for the modes to interact with the surface, but not too close where all of the mode is lost to interaction with the gold nanoparticle solution at the polished surface. If the distance d is decreased to an extreme value such as $d = 1\mu m$ the value of ϕ increases as shown in Figure 5.1c and 5.1d. When ϕ is large enough, more of the LP_{11} mode is contained in the region of interaction shown by the wedge. At this point, both modes experience significant loss and there is no way to distinguish between each loss ratio (R). If the other extreme is considered where d is large enough that the modes no longer interact with the polished surface, the mode profiles are exactly the same as the step index fiber and no loss is achieved for either mode. This also corresponds to the experimental results for the no loss case.

It is now established that the experimental results correspond to the expected results determined by the regions of interaction shown in Figure 5.1. The significance of this research is that groundwork is established for the development of mode-domain sensors and devices utilizing side-polished fiber geometry to interact with the evanescent field of each mode independently. Mode-domain sensors and devices have the potential to advance the field of fiber optics significantly due to the numerous potential applications.

5.1 Applications

The results seen in this study are of particular interest when considering the design of mode-domain sensors and devices. A single fiber can be designed to accommodate both modes and the geometry of the polishing allows access to the evanescent field of each mode independently. For telecommunications, this is significant because it allows the design of devices to promote the field of multimode communication. Multimode fiber is often utilized in short

range, high bandwidth applications since dispersion and attenuation reduce the quality of the signal over long distances. However, multiple modes allow for greater bandwidth because each mode can carry a separate signal in the same fiber. With side-polished fiber, there is significant potential for creating optical devices that could aid the field of multimode fiber optics.

One potential application is a multiplexer. Multimode fiber operation relies on multiplexing to increase bandwidth by either using multiple wavelength channels (wavelength division multiplexing), interleaving channels in a single signal (time division multiplexing), or combining multiple signals into a single spatial domain (spatial division multiplexing). Each of these multiplexing solutions have been developed extensively, but the solution that is most relevant to side-polished fiber is spatial division multiplexing. Simple solutions such as just combining multiple fibers into a single cable have been established, but that increases the size of the fiber cable. A more elegant solution is mode division multiplexing. Since each mode occupies a specific spatial distribution, each mode can carry a unique signal. Since it is established that the spatial distribution of the modes can be influenced independently using a side-polished fiber, it is likely that a multiplexer can be designed by attenuating all but one of the modes propagating in the fiber to access the desired signal. All that would need to be done to create such a device is to identify the unique geometry that allows the propagation of the desired mode and attenuate the other signals by applying an absorbing material such as a gold nanoparticle solution to the polished surface. Not only is this device effective at creating a spatial division multiplexer, but it is a passive device resulting in efficient operation.

The field of fiber optic sensing also has the potential to benefit from mode-dependent side-polished fiber devices. By influencing one of the modes with a certain perturbation and not the other, it is possible to design a wide array of multimode side-polished fiber sensors

that have certain advantages over their single-mode counterparts. One major advantage is the presence of a reference beam and a sensing beam. The reference beam can be used to account for any noise or bias due to bending or interference that is not related to the sensing element. Reducing these errors is vital to improving the sensitivity and accuracy of devices such as fiber optic based refractive index biosensors, distance sensors, and pressure sensors.

5.2 Further Research

There is a significant amount of research to be completed on the topic of few-mode side-polished fiber operation. Numerical simulations would be invaluable in confirming the theoretical expectations to further validate the results of this study. Commercial software is available that can provide computationally intensive results that achieve much more accurate solutions than the theoretical approximations made in this thesis. Even though the approximations presented here can explain the results, more accurate representation of the field distribution for each mode would provide a better understanding of the experimental results.

One area that must be significantly improved is fabrication. The current technique of mechanical polishing is time consuming and tedious. The fiber often breaks due to mechanical strain and weakening at the polished portion of the fiber. Additionally, the accuracy is not ideal as the polishing resolution based on the calibration technique described in Section 3.1 is two micron. In addition, since the behavior of the LP modes was not understood during the fabrication process, the orientation of the LP_{11} mode was not considered. This may have skewed some of the results since the percent transmission would be effected by the orientation of the mode. However, each depth was determined by taking an average of multiple fibers and the results were repeatable. One way to improve the fabrication process

would be to utilize chemical etching with a hydrofluoric acid solution where the etch rate is known. Therefore, depth can be determined more accurately and consistently based off time in the etching solution. This would not rely on transmission percentage which would eliminate the error associated with the orientation of the LP_{11} and significantly simplify the polishing process.

An additional area that could use improvement is the application of the perturbation. The current perturbation using a gold nanoparticle solution is not ideal since the concentration of gold nanoparticles is inconsistent throughout the solution. Over time, the particles settle to the bottom of the container and need to be stirred periodically. This may have led to some unusual results where polishing depths further from the core yielded unexpectedly high loss compared to closer polishing depths. Specifically the 9% transmission case yielded a 32.2% loss for the LP_{01} mode where the 7% and 8% transmission cases were closer to 20%. This discrepancy may be due to the gold nanoparticle solution being more highly concentrated at the point of interaction with the mode. Although not ideal, the loss percentage is less vital than the ratio of loss between each individual mode. The results at each polishing depth were consistent and should not be effected by this possible inconsistency. For future research, it is recommended to use a more consistent perturbation such as a change in refractive index.

The next step to furthering few-mode side-polished fiber devices is to start designing sensors. A refractive index sensor utilizing a sensing mode and reference mode should provide improved resolution and accuracy over previously developed sensors. The reference mode can be used to compensate for noise and perturbations from sources other than the sensing element such as bending. Such improvements have the capability to advance the fields of bio-sensing and material analysis.

Bibliography

[1] T. H. Maiman, "Stimulated Optical Radiation in Ruby," *Nature*, vol. 187, pp. 493–494, 8 1960.

[2] K. C. Kao and G. A. Hockham, "Dielectric-fibre surface waveguides for optical frequencies," *Proceedings of the Institution of Electrical Engineers*, vol. 113, pp. 1151–1158, 7 1966.

[3] G. P. Agrawal, *Fiber-optic communication systems*, vol. 222. John Wiley & Sons, 2012.

[4] E. Udd and W. B. Spillman Jr, *Fiber optic sensors: an introduction for engineers and scientists*. John Wiley & Sons, 2011.

[5] A. D. Kersey, "Optical fiber sensors for permanent downwell monitoring applications in the oil and gas industry," *IEICE transactions on electronics*, vol. 83, no. 3, pp. 400–404, 2000.

[6] A. Alvarez-Herrero, H. Guerrero, and D. Levy, "High-sensitivity sensor of low relative humidity based on overlay on side-polished fibers," *IEEE Sensors Journal*, vol. 4, no. 1, pp. 52–56, 2004.

[7] H.-Y. Lin, W.-H. Tsai, Y.-C. Tsao, and B.-C. Sheu, "Side-polished multimode fiber biosensor based on surface plasmon resonance with halogen light," *Applied optics*, vol. 46, no. 5, pp. 800–806, 2007.

[8] K.-R. Sohn, K.-T. Kim, and J.-W. Song, "Optical fiber sensor for water detection using a side-polished fiber coupler with a planar glass-overlay-waveguide," *Sensors and Actuators A: Physical*, vol. 101, no. 1-2, pp. 137–142, 2002.

[9] B. E. A. Saleh and M. C. Teich, "Fiber Optics," in *Fundamentals of Photonics*, vol. 5, ch. 8, pp. 272–309, John Wiley & Sons, Inc., 1991.

[10] M. Digonnet and H. Shaw, "Analysis of a Tunable Single Mode Optical Fiber Coupler," *IEEE Transactions on Microwave Theory and Techniques*, vol. 30, no. 4, pp. 592–600, 1982.

[11] A. Kumar, D. Uttamchandani, and B. Culshaw, "Relative transmission loss of teand tm-like modes in metal-coated coupler halves," *Electronics Letters*, vol. 25, no. 5, p. 301, 1989.

[12] Z. Ioannidis, I. Giles, and C. Bowry, "Liquid crystal all-fibre optical polariser," *Electronics Letters*, vol. 24, no. 23, p. 1453, 1988.

[13] R. A. Bergh, H. C. Lefevre, and H. J. Shaw, "Single-mode fiber-optic polarizer," *Optics Letters*, vol. 5, p. 479, 11 1980.

[14] S. Markatos, S. Ayres, D. Kreit, A. Kerr, R. C. Youngquist, and I. P. Giles, "Optical Fibre Switch," vol. 0798, p. 376, International Society for Optics and Photonics, 10 1987.

[15] B. F. Lamouroux, A. G. Orszag, B. S. Prade, and J. Y. Vinet, "Continuous laser amplification in a monomode fiber longitudinally pumped by evanescent field coupling," *Optics Letters*, vol. 8, p. 504, 9 1983.

[16] S. A. Newton, K. P. Jackson, and H. J. Shaw, "Optical fiber V-groove transversal filter," *Applied Physics Letters*, vol. 43, pp. 149–151, 7 1983.